Proceedings of the 9th International Symposium on Fluid-Structure Interactions, Flow-Sound Interactions, Flow-Induced Vibration & Noise
July 8-11, 2018, Toronto, Ontario, Canada

FIV2018-47

DRAFT: OPTIMIZATION OF AN UNDERBODY AERODYNAMIC DRAG REDUCTION DEVICE FOR TRAILER TRUCKS

Mohamed Ibrahim
University of Ontario Institute of Technology
Oshawa, ON, Canada

Martin Agelin-Chaab
University of Ontario Institute of Technology,
Oshawa, ON, Canada

ABSTRACT

It is well known that the underbody region of a tractor-trailer is responsible for up to 30% of the aerodynamic drag. This is the highest drag created by any region of a tractor-trailer. Low ground clearance and ice collection are a few of the issues that inhibit the mass market appeal of the underbody drag-reduction devices available on the market. This paper deals with the optimization of a novel concept of an underbody drag reduction device, which combines a ramp and a side skirt. Twelve different device configurations were simulated in order to optimize the angle of the ramp and the side skirt simultaneously. The configurations were evaluated based on the average outlet velocity, mass flow rate and the average outlet pressure of the device. The underbody of a class-8 tractor-trailer model was approximated as a channel where the device configuration was simulated. The studies were conducted using numerical simulation in ANSYS Fluent running the RANS based turbulence model, $k-\omega$ SST. The optimized device configuration was then applied to NASA's Generic Conventional Model (GCM), 1/8th scale class-8 tractor-trailer model, and simulated numerically. The overall drag coefficient was reduced by 4.0%.

NOMENCLATURE

Re	Reynolds number = $\frac{uw}{v}$
V_u	freestream velocity (m/s)
z	lateral distance from the centerline of the model
y	vertical distance from the bottom of the model
x	axial distance from the front of the model

INTRODUCTION

The impact of aerodynamic drag on fuel consumption of heavy vehicles is substantial. Heavy vehicles consume about 25% of all fuel, despite accounting for only 7% of the total vehicles on the road [1]. The US trucking industry alone consumes around 54 billion gallons of fuel per year [2]. At a typical highway speed of 110 km/h, 65% of the total energy used by a heavy vehicle is used to overcome aerodynamic drag [3]. In order to understand the technical challenges faced in aerodynamic drag reduction, it is essential to understand the drag distribution around a trailer truck. The aerodynamic drag distribution around a trailer truck is dominated by four regions, the tractor front face, the tractor-trailer gap, the underbody and the trailer base. The underbody region of the trailer truck is responsible for the highest drag created by any region of a trailer truck; accounting for up to 30% of the aerodynamic drag [4,5]. Thus, focusing on minimizing the drag at the underbody of the vehicle provides the highest drag reduction potential.

Several underbody drag reduction devices have been proposed in the literature, including the undercarriage straight skirt [3,6–9], belly box [8,10], undercarriage wedge skirt [8,11] and the trailer underbody fairing [12]. These underbody devices create a few operational issues that limit their widespread adoption. For example, side skirts limit the ground clearance of heavy vehicle which results in them being damaged from road protrusions, such as speed dumps or loading docks. Additionally, in countries with colder climates, snow and ice collection in the devices increases the vehicle weight. This requires the driver to clear the snow/ice before entering weight stations. More importantly, parasitic drag due to skin friction needs to be mitigated as it can adversely affect the drag of trailer trucks at low speeds. Thus, in

this study a novel underbody drag reduction device concept for trailer trucks is proposed and optimized.

UNDERBODY DEVICE

The underbody device proposed combines the functionality of both an underbody fairing and a side skirt. The underbody fairing is implemented to provide a means for the underbody flow to attach on a surface to reduce recirculation and guide the flow until it exits the underbody of the vehicle. Meanwhile, the side skirt is implemented for three primary reasons. The first being that side skirts have proven to prevent crosswind from disturbing the underbody flow, which provides better drag reduction. Secondly, implementing side skirts that converge can accelerate the underbody flow so that it remains attached at higher ramp angles. Thirdly, converging side skirts can guide the underbody flow away from the trailer wheels, which should aid in further drag reduction. Furthermore, this design has been specifically proposed in order to allow for the collapsibility of the device, thus active drag reduction device. The device concept was designed around NASA's Generic Conventional Model (GCM), a $1/8^{th}$ scale generic class-8 tractor-trailer model. The GCM was chosen as it allowed for the proposed device to be suitable for a wider range of tractor-trailers when compared to a commercial configuration. In addition, as this study is a primary step towards testing the optimized device on a vehicle model, the GCM allows for the simulations to be validated using NASA's experimental data on the model [13,14].

The proposed concept is attached to the underbody of the GCM as shown in Figure 1a. The optimization of the device is done by controlling two dimensions simultaneously, the ramp angle and the side skirt angle (see Fig. 1b,c). This was conducted to ensure that the flow exiting the underbody of the tractor remains attached throughout the trailer length while maintaining a flow velocity that would not adversely affect the wake region i.e. decrease the pressure at the wake. The ramp angle is the angle measured from the ramp to the bottom edge of the side skirt. Meanwhile, the side skirt angle is the angle measured between the side skirt and the trailer side edge. Both of these angles are indicated in Figures 1b and 1c respectively.

a)

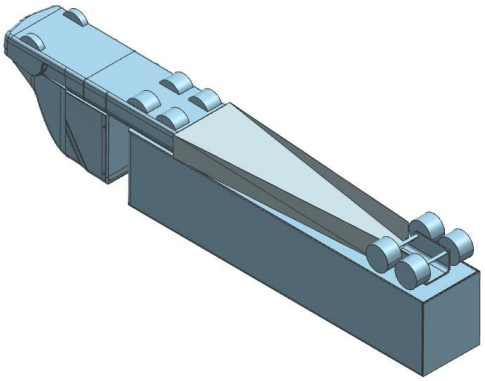

b)

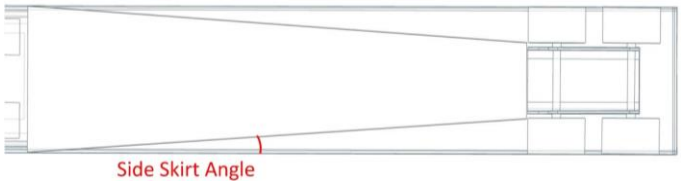

c)

FIGURE 1: a) Proposed underbody drag reduction device attached on the underbody of the GCM b) Bottom view of the device indicating the side skirt angle c) Side view of the device indicating the ramp angle

Twelve different device configurations were evaluated to optimize the proposed concept. The ramp angle was varied between four different configurations (3°, 4°, 5° and 6°) while the side skirt angle was varied between three different configurations (straight side skirt, 3°, and 4°). It is important to note that a straight side skirt would be equivalent to having a side skirt angle of 0°. A summary of the device configurations that were evaluated in this study is shown in Table 1. Each configuration was modeled as a channel in order to reduce the computational time required to evaluate the different configurations. The channel modeled the tractor underbody as well as the interior of the device itself. It is important to note that each domain has a different structure to mimic the interior of the proposed device configuration. For instance, considering the device configuration #12, the location of the channel is highlighted in red (Figure 2b) compared to the GCM (Figure 2a).

In order to determine the highest drag reduction potential of these configurations, the device configurations were assessed in terms of the average outlet velocity, mass flow rate, and outlet pressure. In addition, a channel was modeled to mimic the underbody of the GCM in order to set up a baseline for the twelve device configurations.

TABLE 1: Summary of the different configurations

Configuration Number	Device Description
1	Ramp 3° - Straight Side Skirt
2	Ramp 3° - Side Skirt 3°
3	Ramp 3° - Side Skirt 4°
4	Ramp 4° - Straight Side Skirt
5	Ramp 4° - Side Skirt 3°
6	Ramp 4° - Side Skirt 4°
7	Ramp 5° - Straight Side Skirt
8	Ramp 5° - Side Skirt 3°
9	Ramp 5° - Side Skirt 4°
10	Ramp 6° - Straight Side Skirt
11	Ramp 6° - Side Skirt 3°
12	Ramp 6° - Side Skirt 4°

a)

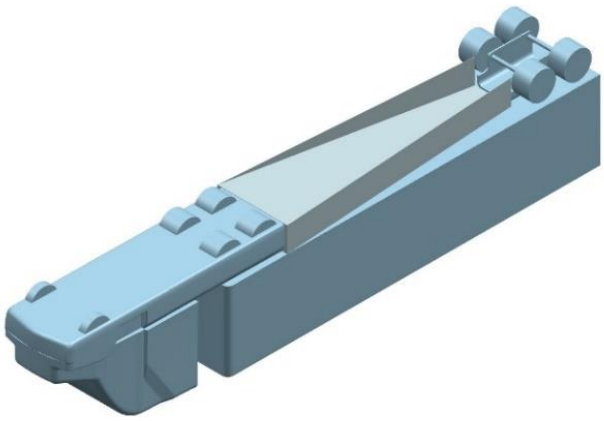

b)

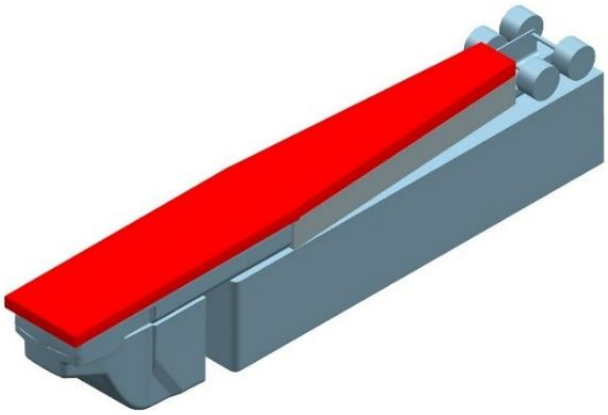

Figure 2: a) GCM with device configuration #12 (Ramp 6° - Side Skirt 4°) and b) the channel location highlighted in red

NUMERICAL SETUP

As 12 different configurations were evaluated, each domain had a different structure to mimic the interior of the proposed device. Figure 3 displays the general details common to all twelve domain configurations used in this study. The first section of the domain models the tractor underbody of the GCM. The tractor wheels were eliminated for simplicity as the primary goal was to evaluate the device concepts and determine which ones had the highest drag reduction potential. The inlet dimensions and the length of the channel were identical for all 12 configurations as these factors were limited by the underbody dimensions of the GCM. The total length of the channel was 1.97 m with the tractor underbody section being 1.02 m in length. The inlet is 0.323 m in width and 0.038 m in height. This height refers to the ground clearance between the tractor and the ground which is modeled to provide a more realistic approximation of the flow in the device.

The simulations were performed at a uniform inlet velocity of 51.45 m/s. This corresponds to a width-based Reynolds number of $Re = 1.1 \times 10^6$. The inlet turbulence intensity was set to 5% [15] and a no-slip stationary plane boundary condition was set for the domain ground. A zero-pressure gradient was specified for the outlet condition. The $k - \omega$ SST turbulence model with wall function was employed for its improved behavior with separating flow and adverse pressure gradients compared to the other turbulence models as well as its reduced computational time and data storage requirements.

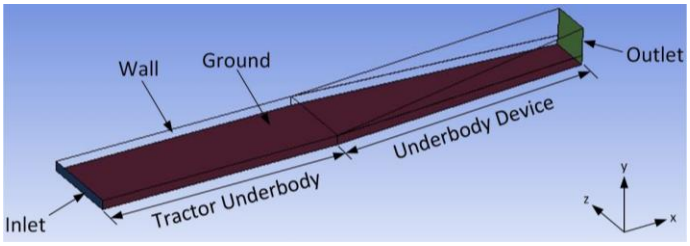

Figure 3: Computational domain

In order to ensure grid independence, three different grids were simulated to determine the effect of the grid on the friction drag inside the channel. The three grid resolutions were a coarse grid of 54064 elements, a medium grid of 104054 elements and a fine grid of 262447 elements. The drag coefficient from the medium and fine grid was compared to the coarse grid. The medium grid had a difference of 0.17 % while the fine grid had a difference of 0.47%. As these differences were minimal, it was decided to use the medium grid for this study to save computational time. A summary of the grid independence study is shown in Table 2.

TABLE 2: Grid Independence Study for the baseline channel

Grid Resolution	Difference in Drag Coefficient
Coarse - 57064	-
Medium - 104054	0.17 %
Fine - 262447	0.47 %

RESULTS AND DISCUSSION

Baseline Channel

Examining the flow through the baseline channel, the flow is comprised of a large recirculation zone that extends throughout the trailer underbody section of the channel; which is evident by the negative flow velocity due to flow separation (Figure 4). The trailer underbody section is the section between the step and the channel exit while the section between the channel entrance is the tractor underbody section. This recirculation zone is caused by the flow separating off the edge of the step, which is essentially an approximation of the tractor underbody. This flow recirculation is responsible for the low-pressure zone in the channel (Figure 5). This low-pressure zone is comparable to the low-pressure region commonly seen at the underbody of a standard tractor-trailer, which is a result of the underbody flow exiting the tractor that separates over the tractors trailing edge. This recirculation approximately covers the entire underbody region of the trailer, causing significant adverse impact on the drag coefficient of the trailer truck mentioned previously.

The average outlet velocity of the flow exiting the channel is 7.77 m/s while the mass flow rate is 0.36 kg/s. This low flow velocity is primarily due to the flow recirculation caused by the separation from the tractor underbody section of the channel. It is important to note that these values are measured y = 0.038 m above the channel ground in order to capture the flow exiting the trailer underbody only.

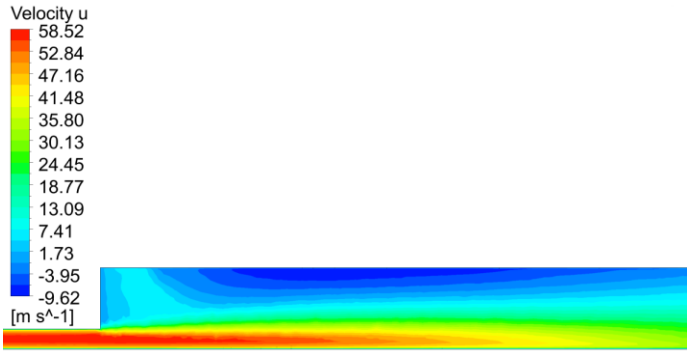

Figure 4: Velocity contour at the centerline of the baseline configuration

Figure 5: Pressure contour at the centerline of the baseline configuration

Channel Optimization

As previously mentioned, twelve device configurations were examined and assessed in terms of three primary metrics; the average outlet velocity, the mass flow rate, and the outlet pressure. Additionally, the velocity contours for each configuration were examined for flow separation. The mass flow rate reflects how much of the flow passing through the channel is attaching to the device and not recirculating. Meanwhile, the outlet pressure is used to inspect how the pressure might affect the flow in the wake of the trailer truck as it exits the device. A high outlet pressure would adversely affect the wake of the vehicle. Based on this study, the top performing device configurations were selected, modeled and simulated on the GCM to determine their effects on the drag coefficient and flow structure around the model.

Examining the flow at device configuration #1 (Ramp 3° - Straight Side Skirt), the flow develops through the tractor underbody section of the channel and attaches to the device all the way to the channel outlet. The flow slows down due to the area expansion of the ramp; with the flow exiting the channel with an average outlet velocity of 14.8 m/s and a mass flow rate of 0.35 kg/s. The average outlet velocity is approximately two times higher compared to the baseline channel. This is attributed to the elimination of flow recirculation as the device configuration provides a smooth transition from the tractor underbody section to the trailer underbody section. The mass flow rate was slightly lower compared to the baseline channel. This is because of the reduction of the surface area at the outlet of the device due to the ramp. Moving on to configuration #2 (Ramp 3° - Side Skirt 3°), the velocity throughout the length of the trailer underbody section is generally higher when compared to configuration #1. This is expected as the converging side skirts accelerate the flow and allow for better flow attachment due to the reduced cross-sectional area. The average outlet velocity increased by approximately two folds to 27.79 m/s compared to configuration #1. In addition, the mass flow rate increased by approximately 16.5% compared to configuration #1. As for configuration #3 (Ramp 3° - Side Skirt 4°), the side skirt angle was increased from 3 to 4 degrees compared to configuration #2. The overall velocity throughout the underbody trailer section was increased compared to the previous two configurations. The average outlet velocity was 36.2 m/s while the mass flow rate was 0.43 kg/s; which are the highest values compared to the previous configurations.

For configurations #4 to 6, the ramp angle was increased from 3 to 4 degrees. Examining device configuration #4 (Ramp 4° - Straight Side Skirt), the flow remained attached throughout the length of the ramp even as the configuration had straight side skirts. The average outlet velocity was 13.1 m/s which is comparable to configuration #1 (Ramp 3° - Straight Side Skirt). The mass flow rate was 0.40 kg/s, an increase of 12.4% compared to configuration #1. Increasing the side skirt angle to 3 degrees in configuration #5 results in an overall increase in the

flow velocity throughout the trailer underbody section of the channel. The average outlet velocity decreased by 19% compared to configuration #2. This is due to the surface area of the channel outlet being larger compared to configuration #2. The mass flow rate increased by 8.9% to 0.439 kg/s compared to configuration #2. Examining configuration #6 (Ramp 4° - Side Skirt 4°), the average outlet velocity was 29.8 m/s while the mass flow rate was 0.475 kg/s. This represents a decrease of 17.6% in the average outlet velocity while the mass flow rate increased by 10% compared to configuration #3.

For configurations #7 – 9, the ramp angle was increased from 4 degrees to 5 degrees. Examining configuration #7 (Ramp 5° - Straight Side Skirt), the flow separates through the trailer underbody section of the channel. This can be seen close to the channel exit, where a negative velocity is evident. This implies that a ramp angle of 5 degrees is just above the threshold of flow separation. The average outlet velocity was 12.2 m/s, which is slightly lower than configuration #4 (Ramp 4° - Straight Side Skirt) which had an average outlet velocity of 13.1 m/s. Meanwhile, the mass flow rate was 0.46 kg/s. Increasing the side skirt angle to 3 degrees, the flow separation that was evident in configuration #7 is eliminated in configuration #8. The average outlet velocity is increased to 18.6 m/s, which is approximately an increase of 52.3 % compared to configuration #7. As for the mass flow rate, it was identical for both configurations. This is plausible as the flow started to separate near the end of the channel for configuration #7, thus the effect of flow separation on the mass flow rate was minor. Further increasing the side skirt angle to 4 degrees resulted in an overall increase in the velocity throughout the trailer underbody section of configuration #9 (Figure 6). The average outlet velocity increased by 33.7% to 24.9 m/s while the mass flow rate increased by 6.5% to 0.49 kg/s compared to configuration #8. Compared to all twelve configurations tested, configuration #9 had the second highest mass flow rate. In addition, this configuration had the second highest ramp angle which allows for a higher ground clearance compared to the other device configurations.

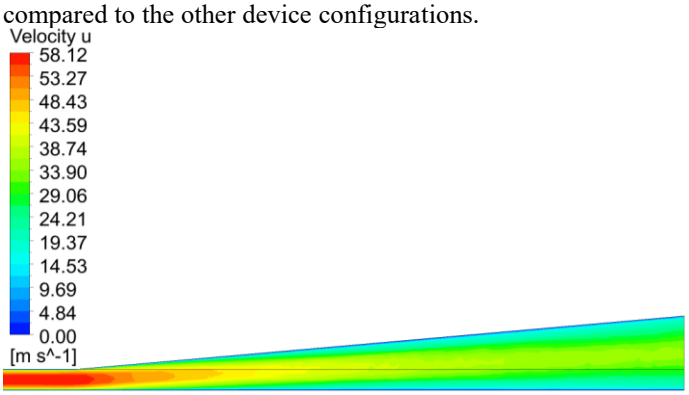

Figure 6: Velocity contour at the centerline of device configuration #9 (Ramp 5° - Side Skirt 4°)

Finally, for configurations #10 to 12, the ramp angle was increased to 6 degrees. This resulted in the flow separation occurring much sooner when compared to configuration #7 (Ramp 5° - Straight Side Skirt). This is expected due to the increase in the ramp angle. The average outlet velocity was 9.9 m/s, which is the lowest outlet velocity recorded between all twelve device configurations. This drastic decrease in out flow velocity is attributed to the flow separating and recirculating at approximately halfway through the trailer underbody section of the channel. Moving onto configuration #11 (Ramp 6° - Side Skirt 3°), the converging side skirts eliminated the flow separation seen in the previous configuration. The converging side skirts increase the flow velocity, which in turn energizes the flow allowing it to attach to higher ramp angles. The average outlet velocity was 15.9 m/s while the mass flow rate was 0.46 kg/s. Finally, for configuration #12 (Ramp 6° - Side Skirt 4°) the mass flow rate increased by approximately 8.7% compared to configuration #11. This configuration had the highest mass flow rate compared to all the other device configurations. Additionally, this configuration had the highest ramp angle which allows for a higher ground clearance compared to the other device configurations. The flow field of this configuration is shown in Figure 7. A summary of all the results discussed for the twelve device configurations is shown in Table 3.

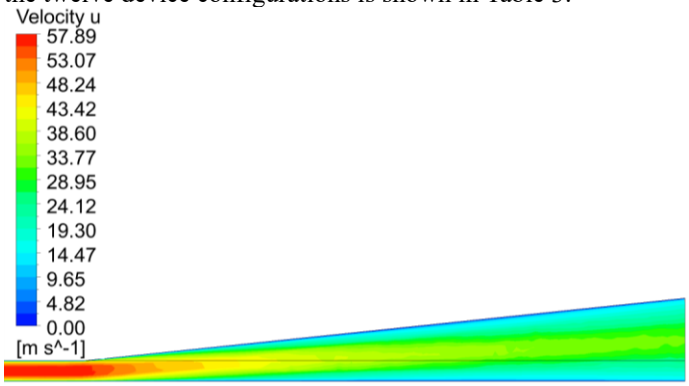

Figure 7: Velocity contour at the centerline of device configuration #12 (Ramp 6° - Side Skirt 4°)

In summary, the highest two configurations in terms of mass flow rate were configurations #12 and configuration #9 with a mass flow of 0.50 kg/s and 0.49 kg/s respectively. As for the average outlet velocity, configurations #3 and #6 had the highest average outlet velocity of 36.1 m/s and 29.8 m/s respectively. Flow separation was evident in configurations #7 and #10, thus they were eliminated. Based on these results, it was concluded that the optimum two configurations were configurations #12 (Ramp 6° - Side Skirt 4°) and configuration #9 (Ramp 5° - Side Skirt 4°) as they provided the highest mass flow rate exiting the device; which signifies that more of the bulk flow is attaching to the device and guided to the end of the channel when compared to the baseline channel were the flow was recirculating at the trailer underbody region. Additionally, the outlet pressure of these two configurations was close to negligible at 0.4 Pa. Thus, these device configurations would not have an adverse impact on the wake of the trailer truck. These two configurations were simulated on the GCM in another study, were device configuration #12 reduced the overall drag coefficient by 4.1 % while configurations #9 resulted in a drag reduction of 3.3 %

[16]. A drag reduction of 4% would translate to fuel saving of up to $2600 per year for a single tractor-trailer.

TABLE 3: Summary of the results comparing the average outlet velocity, mass flow rate and average outlet pressure of all 12 device configurations

Configuration Number	Average Outlet Velocity (m/s)	Mass Flow Rate (kg/s)	Average Outlet Pressure (Pa)
Baseline	7.77	0.356	-2.59
1	14.80	0.346	-2.21
2	27.80	0.403	-0.56
3	36.16	0.432	2.62
4	13.10	0.400	-1.19
5	22.54	0.439	-0.68
6	29.78	0.475	1.29
7	12.23	0.460	-2.36
8	18.63	0.460	-0.67
9	24.91	0.490	0.39
10	9.86	0.450	-3.52
11	15.85	0.460	-0.73
12	21.41	0.500	0.39

CONCLUSION

In this study, a novel underbody drag reduction device is optimized. The underbody device consists of a combination of a ramp and a side skirt. The device was optimized by controlling two dimensions simultaneously, the ramp angle and the side skirt angle. Twelve different device configurations were tested; were the ramp angle was varied between four different configurations (3°, 4°, 5° and 6°) while the side skirt angle was varied between three different configurations (straight side skirt, 3°, and 4°). These configurations were compared to a baseline channel that mimicked the underbody of a trailer truck.

The optimum two configurations were concluded to be configurations #12 and #9. These configurations were chosen primarily because they provided the highest mass flow rate at the outlet of the device while maintaining a high exit velocity that does not affect the outlet pressure significantly.

ACKNOWLEDGMENTS

Financial support of this work by the Natural Science and Engineering Research Council of Canada is gratefully acknowledged.

REFERENCES

[1] ORNL, 2013, *Transportation Energy Data Book*.

[2] American Trucking Associations, 2015, "Reports, Trends & Statistics" [Online]. Available: http://www.trucking.org/News_and_Information_Reports_Industry_Data.aspx.

[3] McCallen, R., Salari, K., Ortega, J., DeChant, L. J., Hassan, B., Roy, C. J., Pointer, W. D., Browand, F., Hammache, M., Hsu, T.-Y., Leonard, A., Rubel, M., Chatalain, P., Englar, R., Ross, J., Satran, D., Heineck, J. T., Walker, S., Yaste, D., and Storms, B., 2004, "DOE's Effort to Reduce Truck Aerodynamic Drag - Joint Experiments and Computations Lead to Smart Design," 34th AIAA Fluid Dyn. Conf. Exhib., (July), pp. 1–16.

[4] Drollinger, R., 1987, "Heavy Duty Truck Aerodynamics," SAE Tech. Pap. Ser.

[5] Sovran, G., 1978, *Aerodynamic Drag Mechanisms of Bluff Bodies and Road Vehicles*, Springer.

[6] Salari, K., Ortega, J., and Castellucci, P., 2004, "Computational Prediction of Aerodynamic Forces for a Simplified Integrated Tractor-Trailer Geometry," *34th AIAA Fluid Dynamics Conference and Exhibit*, American Institute of Aeronautics and Astronautics.

[7] Buil, R. M., and Herrer, L. C., 2009, "Aerodynamic Analysis of a Vehicle Tanker," J. Fluids Eng., **131**(4), pp. 41204–41217.

[8] Cooper, K. R., and Leuschen, J., 2005, "Model and Full-Scale Wind Tunnel Tests of Second-Generation Aerodynamic Fuel Saving Devices for Tractor-Trailers."

[9] Tooren, M. V., and Raemdonck, G. V., 2009, "A Practical Scientific Approach For Aerodynamic Truck Design," Proc. Euromech Colloq. 509 Extern. Aerodyn. Railw. Veh. Truck. Buses Cars, pp. 293–303.

[10] Leuschen, J., and Cooper, K. R., 2006, "Full-Scale Wind Tunnel Tests of Production and Prototype, Second-Generation Aerodynamic Drag-Reducing Devices for Tractor-Trailers," SAE Tech. Pap., (2006-01–3456).

[11] Ortega, J., and Salari, K., 2004, "An Experimental Study of Drag Reduction Devices for a Trailer Underbody and Base," 34th AIAA Fluid Dyn. Conf. Exhib., (July), pp. 1–15.

[12] Ortega, J., and Salari, K., 2008, "Investigation of a Trailer Underbody Fairing for Heavy Vehicle Aerodynamic Drag Reduction," Heavy Veh. Syst. Optim. Progr. - FY 2008 Annu. Rep., pp. 241–250.

[13] Storms, B., Satran, D., Heineck, J., and Walker, S., 2004, "A Study of Reynolds Number Effects and Drag-Reduction Concepts on a Generic Tractor-Trailer," *34th AIAA Fluid Dynamics Conference and Exhibit*, American Institute of Aeronautics and Astronautics.

[14] Storms, B., Satran, D. R., Heineck, J. T., and Walker, S. M., 2006, *A Summary of the Experimental Results for a Generic Tractor-Trailer in the Ames Research Center 7-by 10-Foot and 12-Foot Wind Tunnels*, Moffett Field, CA.

[15] Lauwers, K., 2009, "Computational and Experimental Analysis of Trailer Shape Modifications for Drag Reduction," Delft University of Technology.

[16] Ibrahim, M., and Agelin-Chaab, M., 2018, "Investigation and Development of Underbody Aerodynamic Drag Reduction Devices for Trailer Trucks," SAE Tech. Pap.